

Accuracy analysis of Dual Active Bridge simulations under different integration methods

1st Gabriele Arena 

Institute for Technical Physics (ITEP)
Karlsruhe Institute of Technology (KIT)
Karlsruhe, Germany

2nd Dmitri Vinnikov 

Power Electronics Research Group
Tallinn Institute of Technology (TalTech)
Tallinn, Estonia

3rd Andrii Chub 

Power Electronics Research Group
Tallinn Institute of Technology (TalTech)
Tallinn, Estonia

4th Giovanni De Carne 

Institute for Technical Physics (ITEP)
Karlsruhe Institute of Technology (KIT)
Karlsruhe, Germany

Abstract—One of the biggest challenge in the power electronics field is the simulation of power converters. Computer simulations and real-time simulations are really important in this field because they allow to save money during the prototyping stage and to make the entire process more efficient by predicting possible malfunctions already in the design stage. This paper introduces the impact of using different integration methods for solving the differential equations of power converters on the accuracy of the simulation. In particular, the paper focus on one of the most adopted DC-DC converter topology for automotive and microgrid applications, which is the Dual Active Bridge.

Index Terms—Digital real time simulation, dual active bridge, integration methods.

I. INTRODUCTION

Power electronics have known a large growth over the years in several fields, such as automotive industry, smart grids and aerospace, due to its advanced power controllability. Power converters can be used every time a power conversion is required, such as battery interface or motor drives. The development process of a power converter must involve planning, design and testing stages. One of the major focus in the design stage of a power converter has been the creation of mathematical models for accurate modelling in simulation, particularly for real time applications [1]. However, few papers address the problem of integration methods and time steps to solve the ordinary differential equations (ODE) of these circuits. An accurate simulation is important because allows to find out any malfunction of the converter already in the design stage rather than at the end of the development process, especially if working with real-time simulations [2], [3].

This paper has studied how solvers solve the mathematical model of a well-known DC-DC isolated converter topology, Dual Active Bridge (DAB), under different integration

methods and it has studied the accuracy of each of them with respect to a reference simulation. The DAB has been used for several applications, such as, interface of photovoltaic systems, on-board and off-board battery charging of electric vehicles, interface of battery energy storage systems (BESSs) and development of solid state transformers (SSTs) [4]–[10]. A comparison of solvers for simulations of photovoltaic systems has already been carried out in [11], but taking into account only three solvers and without the related mathematical explanation. Moreover, [12] explains numerical methods to solve differential equations, but without showing specific results for any particular power converter. In [7] and [13], respectively a traditional two-port DAB and a four-port DAB have been investigated through real-time simulations. However, even these works do not carry out any study regarding the accuracy of the simulation for different solver settings. A paper that address the problem of the accuracy for different solver methods is [14]. However, the focus here is only on discrete-time model of induction machines, and no inverters for the motor drives are considered. In [15] instead, a novel multirate integration method is compared with single-rate approaches for motor drives applications. Here, a system with a synchronous machine and a rectifier system has been taken into account. However, even though the multi-rate simulation approach works properly for the simulation of the entire system, the rectifier has not been considered alone but as a part of a motor drive application and such kind of multi-rate approaches are usually not suitable for digital real-time simulators.

The rest of this work is divided as follows. The second paragraph deals with the working principle of the DAB; the third chapter explains the main integration methods that can be used in simulations at fixed time-step; the fourth paragraph is about the simulation results for different time steps and integration methods and finally the fifth chapter is about the conclusions and future improvements of this work.

This work was supported by the Helmholtz Association under the program "Energy System Design". The work of Giovanni De Carne was supported by the Helmholtz Association within the Helmholtz Young Investigator Group "Hybrid Networks" (VH-NG-1613). This project has also received funding from the European Union's Framework Programme for Research and Innovation, Horizon 2020 (2014-2020), under the Marie Skłodowska-Curie Grant Agreement No. 955614.

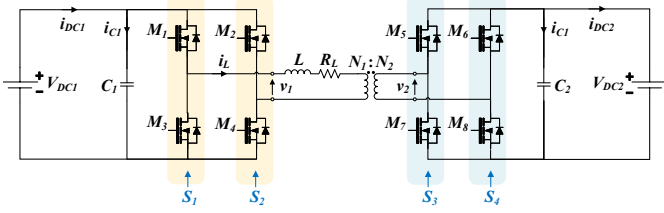


Fig. 1: Dual active bridge topology.

II. DUAL ACTIVE BRIDGE WORKING PRINCIPLE

As already discussed in the introduction, the DAB has been considered a suitable choice for a large number of applications. The features that make this converter appealing as power conversion technology are: bidirectional power flow, galvanic isolation, high power density, wide voltage gain range and capability to perform soft-switching through proper modulation techniques, which improves a lot the efficiency of this converter [4]–[6]. As shown in Fig. 1, the DAB is made of two full bridges, two filter capacitors, one high-frequency transformer and one inductor used to regulate the maximum power exchanged by the converter. The converter can be modulated through different modulation methods, but the one considered in this paper is the most common one, the so called phase shift modulation, in which a phase shift φ is used between the modulation of the two full bridges to reach a certain power transfer. The latter is given by the following formula:

$$P = \frac{nV_{DC1}V_{DC2}\varphi(\pi - |\varphi|)}{2\omega_s\pi L}, \quad \forall -\pi \leq \varphi \leq \pi \quad (1)$$

where $n = \frac{N_1}{N_2}$ is the turn ratio of the transformer, V_{DC1} and V_{DC2} are the first and secondary side voltages, $\omega_s = \pi f_s$ is the angular velocity associated to the switching frequency f_s of the converter and L is the inductor of the converter. The maximum power transfer of the converter is obtained for $\varphi = \pm\frac{\pi}{2}$, where the sign determines the direction of the power flow. The phase shift modulation and the inductor waveforms derived from it are shown in Fig. 2. Here, it is possible to notice the phase shift between the switching signals of the two full bridges of the DAB, which in turn divide the operating period of the converter in 4 sub-intervals, where the mean value of the inductor current is theoretically 0 in steady state.

In this paper, a DAB with a resistive load rather than a voltage source on the second side has been considered. Furthermore, in order to define the analytical model of DAB, it is possible to neglect the first side capacitor. In such a way, the system is only described by the differential equations of the inductor current and second side voltage capacitor. The first one is given as follows:

$$\frac{di_L(t)}{dt} = \frac{V_{dc1}}{L}T_1(t) - \frac{N_1}{N_2} \frac{v_{C2}(t)}{L}T_2(t) - \frac{R_L}{L}i_L(t), \quad (2)$$

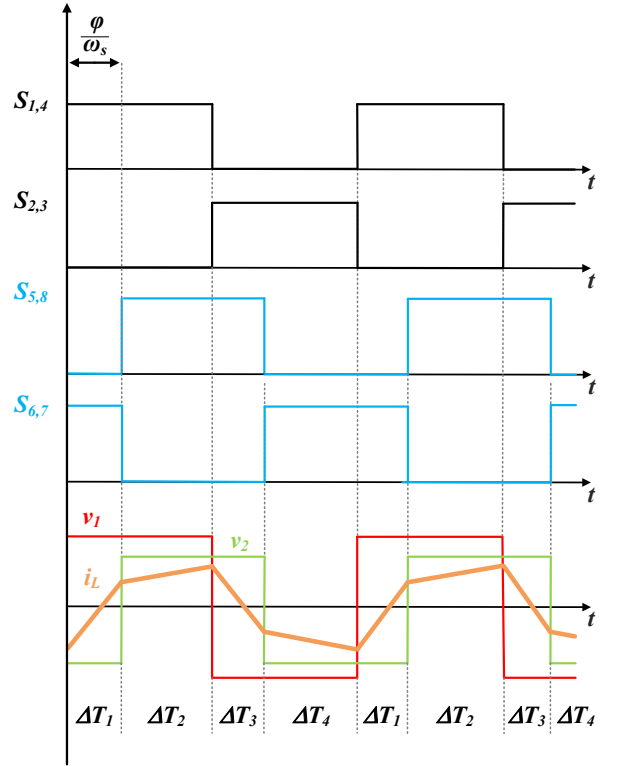


Fig. 2: Dual active bridge waveforms.

whereas the voltage capacitor equation is the following:

$$\frac{dv_{C2}(t)}{dt} = \frac{N_1}{N_2} \frac{i_L(t)}{C_2}T_2(t) - \frac{v_{C2}(t)}{R_{load}C_2}, \quad (3)$$

with $T_1(t) = S_{1,4}(t) - S_{2,3}(t)$ and $T_2(t) = S_{5,8}(t) - S_{6,7}(t)$.

III. INTEGRATION METHODS

This paragraph is about the numerical integration methods used in simulations to solve the dynamic equations of the DAB. Only fixed step integration methods are discussed here, because in digital real-time simulators like OPAL-RT only these methods can be employed. The chosen integration methods range from the first to the fourth order and are respectively Euler, Heun, Bogacki-Shampine and Runge-Kutta [12], [14], [15].

A. Euler Method

The Euler method is a first order integration method to solve differential equations, where the local error is proportional to the square of the time step and the cumulative error is proportional to the time step.

$$y_{n+1} = y_n + \Delta t \cdot F(t_n, y_n) + O(h^2), \quad (4)$$

where y_n and y_{n+1} are respectively the values of the state variables at the current and next time step, Δt is the time step, $F(t_n, y_n)$ is the system of differential equations to be

solved and $O(h^2)$ means that this method has a first-order accuracy.

B. Heun's Method

The second order integration method is called Heun's method and it calculates the next value of the differential equation by calculating first an intermediate value. The Heun's integration method is given as follows:

$$\tilde{y}_{n+1} = y_n + \Delta t \cdot F(t_n, y_n) \quad (5)$$

$$y_{n+1} = y_n + \frac{\Delta t}{2} [F(t_n, y_n) + F(t_{n+1}, \tilde{y}_{n+1})] + O(h^3) \quad (6)$$

where \tilde{y}_{n+1} is an intermediate value, $F(t_n, \tilde{y}_{n+1})$ is the differential equation calculated for \tilde{y}_{n+1} , and $O(h^3)$ means that a second order integration method has been used to integrate the differential equations.

C. Bogacki-Shampine method

Bogacki-Shampine method is a third order method to solve differential equations. It is given as follows:

$$\begin{cases} y_{n+1} = y_n + \frac{2}{9}\Delta t \cdot k_1 + \frac{1}{3}\Delta t \cdot k_2 + \frac{4}{9}\Delta t \cdot k_3 + O(h^4) \\ k_1 = F(t_n, y_n) \\ k_2 = F(t_n + \frac{1}{2}\Delta t, y_n + \frac{1}{2}\Delta t \cdot k_1) \\ k_3 = F(t_n + \frac{3}{4}\Delta t, y_n + \frac{3}{4}\Delta t \cdot k_2) \end{cases} \quad (7)$$

where $O(h^4)$ means that this is a third order integration method.

D. Runge-Kutta Method

Finally, the 4th order integration method is the Runge-Kutta method. It is defined as follows:

$$\begin{cases} y_{n+1} = y_n + \frac{\Delta t}{6} \cdot (k_1 + 2k_2 + 2k_3 + k_4) + O(h^5) \\ k_1 = F(t_n, y_n); \\ k_2 = F(t_n + \frac{1}{2}\Delta t, y_n + \frac{1}{2}\Delta t \cdot k_1); \\ k_3 = F(t_n + \frac{1}{2}\Delta t, y_n + \frac{1}{2}\Delta t \cdot k_2); \\ k_4 = F(t_n + \Delta t, y_n + \Delta t \cdot k_3); \end{cases} \quad (8)$$

where $O(h^5)$ means that the Runge-Kutta method is a fourth order integration method. All the methods previously explained can be obtained as particular cases of the Runge-Kutta method.

IV. SIMULATION RESULTS

The simulations in this chapter have been carried out by using Matlab as development environment. This chapter is divided into two paragraphs, respectively the comparison of the results of different integration methods with the ode45 Matlab solver as reference; and the analysis of the computational time required by each solver to run the simulation. Two DAB have been considered to show the different results that an integration method can achieve in terms of accuracy when the switching frequency changes.

Their parameters are reported in Tab. I. The only differences between these two configurations are the switching frequency, respectively 10 kHz and 1 kHz, and the inductor values, respectively 400 μ F and 4 mH. The inductor values change together with the switching frequency in order to keep the same power rating. In fact, power and voltages have been chosen according to home battery charger applications for electric vehicles, whereas the inductor value is obtained from (1) by substituting 90° to φ , because this is the maximum phase shift angle allowed for a DAB working in open loop.

TABLE I: Converter specifications

Converter specifications			
Name	Value	Name	Value
P	5 kW	C	470 μ F
V_{DC1}	400 V	R_{load}	110 Ω
N_1	8	N_2	15
f_{sw1}	10 kHz	L_1	400 μ H
f_{sw2}	1 kHz	L_2	4 mH

A. Comparison of the results

Fig. 3 compares the output voltage of the first configuration of DAB made by the Runge-Kutta method at different time steps and the ode45 result. Fig. 4 makes the same comparison for the inductor current. In both these figures, it is possible to notice that the improvement in terms of accuracy is higher when passing from 10 μ s to 1 μ s time step, than when passing from 1 μ s to 100 ns. So, as already expected, the more the time step decreases, the less improvement it is achieved in terms of accuracy. This means that, in specific conditions, it is possible to choose even a time step in the order of μ s in power electronics simulations if the considered application does not require a high accuracy. Achieving a good compromise between accuracy and computational time is important especially when working with real time simulations, where the small is the time step and the higher is the risk of overruns, which compromise the validity of such simulations.

Fig. 5 and 6 compare the capacitor voltage and inductor current of the first configuration of DAB for the different integration methods proposed in this paper at a time step of 100 ns with the ode45 result. The same comparison has been made in Fig. 7 and Fig. 8 at a time step of 1 μ s. From both these time steps, it is possible to notice that the Bogacki-Shampine method approximates the system better. In particular, the output voltage achieved from the Bogacki-Shampine method and from the ode45 solver are almost superimposed at both 100 ns and 1 μ s.

Fig. 9 and 10 show capacitor voltage and inductor current of the second configuration of DAB for all the integration methods discussed at a time step of 100 ns and ode45. This time, not only are the Bogacki-Shampine results almost superimposed on the ode45 results, but also the Euler results are. So, while the Runge-Kutta method was better than Euler for approximating the first configuration of DAB, Euler is more suitable for the second one. This result means

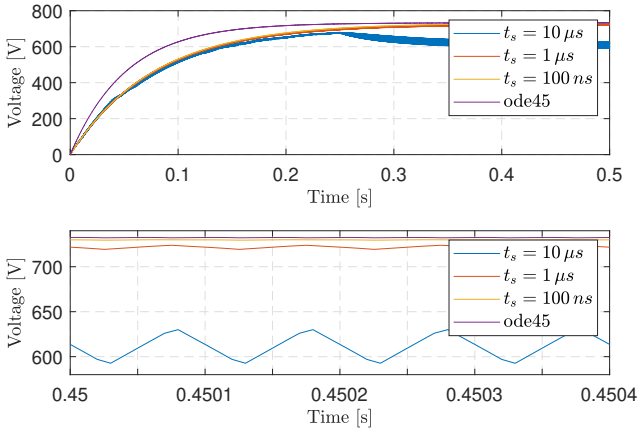


Fig. 3: Output voltage of the first configuration of DAB. Comparison between Runge-Kutta at different integration steps and ode45.

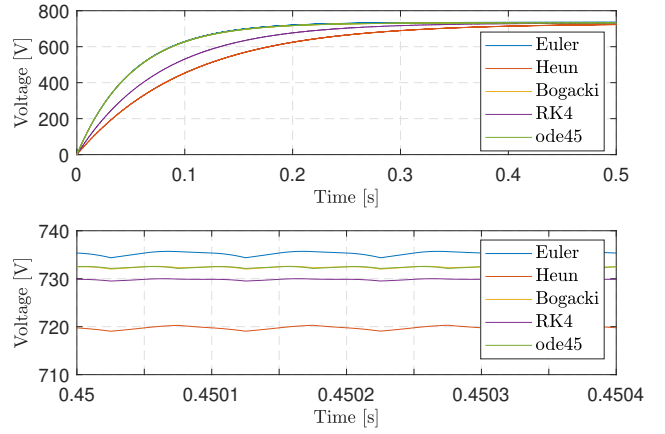


Fig. 5: Output voltage of the first configuration of DAB. Comparison between different solvers at $t_s = 100$ ns.

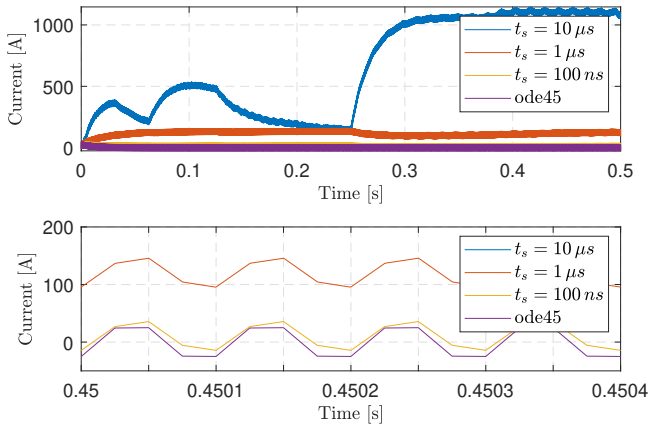


Fig. 4: Inductor current of the first configuration of DAB. Comparison between Runge-Kutta at different integration steps and ode45.

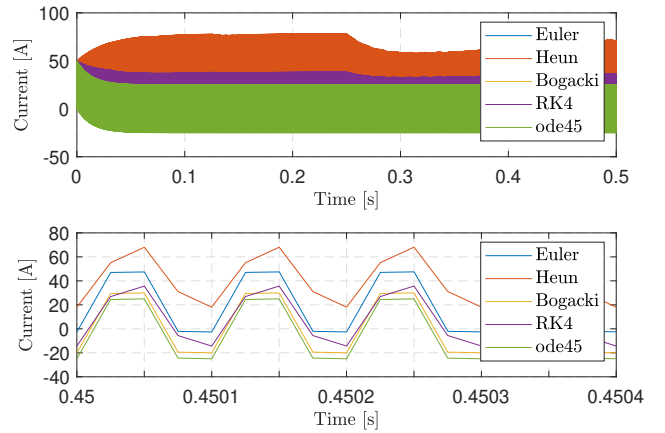


Fig. 6: Inductor current of the first configuration of DAB. Comparison between different solvers at $t_s = 100$ ns.

that different parameters, even for the same converter and differential equations, can lead to a different choice of the integration method.

B. Computational time

The computational time has been measured on a laptop with an Intel(R) Core(TM) i7-10510U CPU with 1.80 GHz base clock frequency and 16 GB of RAM, whereas the operating system is Windows 10 Enterprise. Tab. II and III contain the minimum and maximum simulation duration for both DAB configurations, respectively at $t_s = 100$ ns and $t_s = 1 \mu s$. These results show that the Euler method can be more appropriate when the computational time is a key factor, such as real-time simulations. However, it is always important to achieve a good compromise between the accuracy and the computational effort, because a fast but not accurate simulation can give some wrong information about the system itself. Another detail to observe is that the ode45 solver is a

variable step solver. So, it is faster than the other integration methods for small time steps but slower for high time steps.

TABLE II: Simulation duration for $t_s = 100$ ns

Simulation duration		
Int. method	min. sim. time (s)	max. sim. time (s)
Euler	7.553	8.371
Heun	21.683	22.874
Bogacki-Shampine	21.086	22.738
Runge-Kutta	27.878	30.360
ode45	12.366	17.950

V. CONCLUSIONS

This paper has dealt with the problem of solving the ODE of the DAB by using different integration methods and

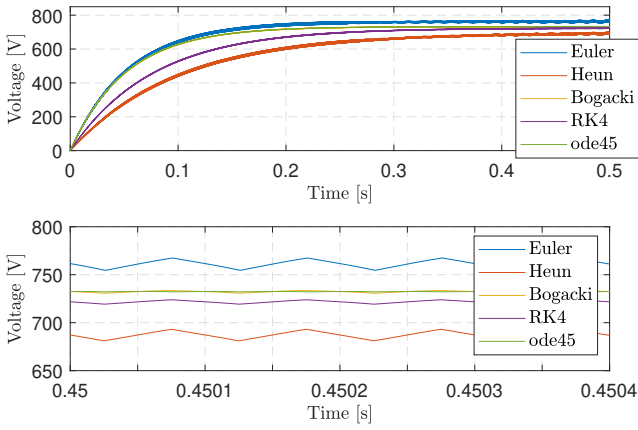


Fig. 7: Output voltage of the first configuration of DAB. Comparison between different solvers at $t_s = 1 \mu\text{s}$.

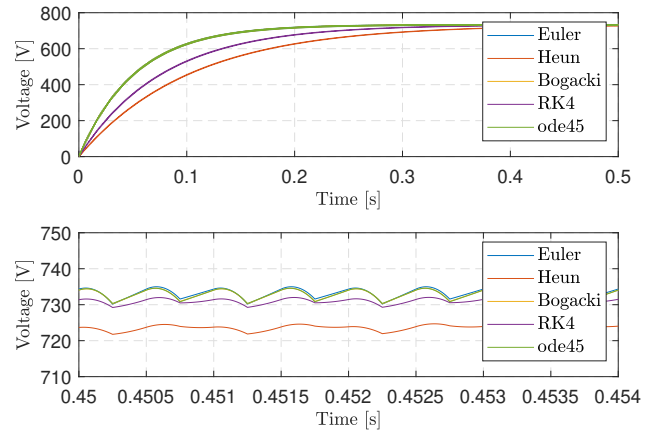


Fig. 9: Output voltage of the second configuration of DAB. Comparison between different solvers at $t_s = 100 \text{ ns}$.

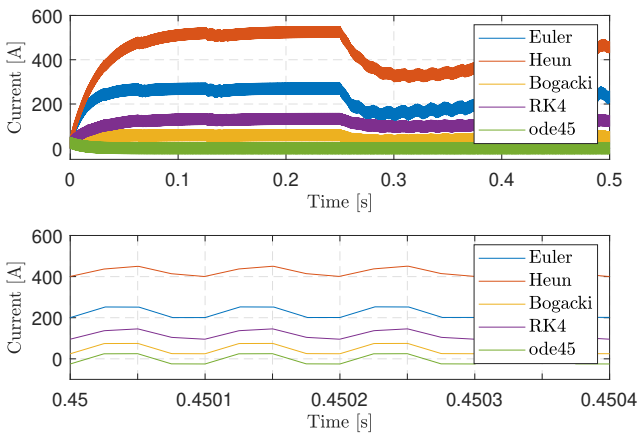


Fig. 8: Inductor current of the first configuration of DAB. Comparison between different solvers at $t_s = 1 \mu\text{s}$.

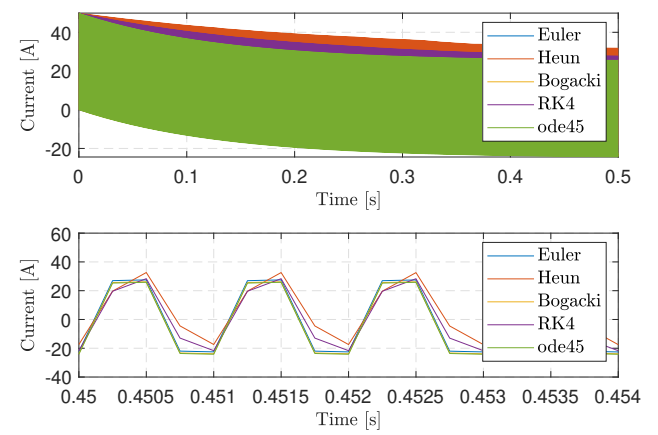


Fig. 10: Inductor current of the second configuration of DAB. Comparison between different solvers at $t_s = 100 \text{ ns}$.

TABLE III: Simulation duration for $t_s = 1 \mu\text{s}$

Simulation duration		
Int. method	min. sim. time (s)	max. sim. time (s)
Euler	0.836	0.963
Heun	2.283	2.756
Bogacki-Shampine	2.155	2.870
Runge-Kutta	2.801	3.319
ode45	12.366	17.950

different time steps. An important result that has been achieved is that different parameters of the same converter topology, the frequency and inductor values in this case, can lead to different results in terms of accuracy of different integration methods. For example, the Euler method is able to give a better approximation than the Runge-Kutta method for the DAB with the switching frequency of 1 kHz and viceversa Runge-Kutta

results better with the one that switches at 10 kHz, despite the same choice of voltage and power ratings. Another point is the necessity to choose the integration method based on the requirements in terms of simulation duration, especially in real-time simulations. The future work should be able to give some further indications for the use of integration methods in power electronics simulations to find a suitable compromise between accuracy and speed of simulation.

REFERENCES

- [1] G. De Carne et al., "On Modeling Depths of Power Electronic Circuits for Real-Time Simulation – A Comparative Analysis for Power Systems," in *IEEE Open Access Journal of Power and Energy*, vol. 9, pp. 76-87, 2022, doi: 10.1109/OAJPE.2022.3148777.
- [2] A. Benigni, T. Strasser, G. De Carne, M. Liserre, M. Cupelli and A. Monti, "Real-Time Simulation-Based Testing of Modern Energy Systems: A Review and Discussion," in *IEEE Industrial Electronics Magazine*, vol. 14, no. 2, pp. 28-39, June 2020, doi: 10.1109/MIE.2019.2957996.
- [3] G. De Carne et al., "Which Deepness Class Is Suited for Modeling Power Electronics?: A Guide for Choosing the Right Model for Grid-Integration Studies," in *IEEE Industrial Electronics Magazine*, vol. 13, no. 2, pp. 41-55, June 2019, doi: 10.1109/MIE.2019.2909799.

- [4] B. Zhao, Q. Song, W. Liu and Y. Sun, "Overview of Dual-Active-Bridge Isolated Bidirectional DC–DC Converter for High-Frequency-Link Power-Conversion System," in *IEEE Transactions on Power Electronics*, vol. 29, no. 8, pp. 4091-4106, Aug. 2014, doi: 10.1109/TPEL.2013.2289913.
- [5] S. Shao et al., "Modeling and Advanced Control of Dual-Active-Bridge DC–DC Converters: A Review," in *IEEE Transactions on Power Electronics*, vol. 37, no. 2, pp. 1524-1547, Feb. 2022, doi: 10.1109/TPEL.2021.3108157.
- [6] F. Krismer and J. W. Kolar, "Accurate Small-Signal Model for the Digital Control of an Automotive Bidirectional Dual Active Bridge," in *IEEE Transactions on Power Electronics*, vol. 24, no. 12, pp. 2756-2768, Dec. 2009, doi: 10.1109/TPEL.2009.2027904.
- [7] G. Arena, G. Aiello, G. Scelba, M. Cacciato and F. Gennaro, "A Cost-Effective Hardware in the Loop Implementation of Dual Active Bridge for Fast Prototyping of Electric Vehicles Charging Controls," 2021 23rd European Conference on Power Electronics and Applications (EPE'21 ECCE Europe), 2021, pp. P.1-P.10, doi: 10.23919/EPE21ECCEEurope50061.2021.9570652.
- [8] M. Liserre, G. Buticchi, M. Andresen, G. De Carne, L. F. Costa and Z. -X. Zou, "The Smart Transformer: Impact on the Electric Grid and Technology Challenges," in *IEEE Industrial Electronics Magazine*, vol. 10, no. 2, pp. 46-58, June 2016, doi: 10.1109/MIE.2016.2551418.
- [9] S. Pugliese, G. Buticchi, R. A. Mastromauro, M. Andresen, M. Liserre and S. Stasi, "Soft-Start Procedure for a Three-Stage Smart Transformer Based on Dual-Active Bridge and Cascaded H-Bridge Converters," in *IEEE Transactions on Power Electronics*, vol. 35, no. 10, pp. 11039-11052, Oct. 2020, doi: 10.1109/TPEL.2020.2977226.
- [10] G. Buticchi, D. Barater, L. F. Costa and M. Liserre, "A PV-Inspired Low-Common-Mode Dual-Active-Bridge Converter for Aerospace Applications," in *IEEE Transactions on Power Electronics*, vol. 33, no. 12, pp. 10467-10477, Dec. 2018, doi: 10.1109/TPEL.2018.2801845.
- [11] E. Kaufhold, J. Meyer, P. Schegner, A. S. Abdelsamad and J. M. A. Myrzik, "Comparison of solvers for time-domain simulations of single-phase photovoltaic systems," 2020 International Conference on Smart Grids and Energy Systems (SGES), 2020, pp. 550-555, doi: 10.1109/SGES51519.2020.00103.
- [12] F. Li et al., "Review of Real-time Simulation of Power Electronics," in *Journal of Modern Power Systems and Clean Energy*, vol. 8, no. 4, pp. 796-808, July 2020, doi: 10.35833/MPCE.2018.000560.
- [13] M. L. Mendola, M. di Benedetto, A. Lidozzi, L. Solero and S. Bifaretti, "Four-Port Bidirectional Dual Active Bridge Converter for EVs Fast Charging," 2019 IEEE Energy Conversion Congress and Exposition (ECCE), 2019, pp. 1341-1347, doi: 10.1109/ECCE.2019.8912252.
- [14] J. Cordier, S. Klass and R. Kennel, "A Discrete-Time Model of Induction Machines Including Winding Distribution Harmonics," 2019 IEEE 13th International Conference on Power Electronics and Drive Systems (PEDS), 2019, pp. 1-7, doi: 10.1109/PEDS44367.2019.8998799.
- [15] S. D. Pekarek et al., "An efficient multirate Simulation technique for power-electronic-based systems," in *IEEE Transactions on Power Systems*, vol. 19, no. 1, pp. 399-409, Feb. 2004, doi: 10.1109/TPWRS.2003.821452.